Analytic formulations for one-dimensional decay of rectangular homoepitaxial islands during coarsening on anisotropic fcc (110) surfaces

Chi-Jen Wang,[1] Yong Han,[2,*] Holly Walen,[3] Selena M. Russell,[3,†] Patricia A. Thiel,[3,4,5] and James W. Evans[1,2,5]

[1]*Department of Mathematics, Iowa State University, Ames, Iowa 50011, USA*
[2]*Department of Physics and Astronomy, Iowa State University, Ames, Iowa 50011, USA*
[3]*Department of Chemistry, Iowa State University, Ames, Iowa 50011, USA*
[4]*Department of Materials Science and Engineering, Iowa State University, Ames, Iowa 50011, USA*
[5]*Ames Laboratory—U.S. Department of Energy, Iowa State University, Ames, Iowa 50011, USA*

Submonolayer homoepitaxial fcc (110) systems display behavior reflecting strong anisotropy at lower temperatures, including one-dimensional decay during Ostwald ripening of rectangular islands maintaining constant width in the $\langle 001 \rangle$ direction. To appropriately describe this behavior, we first develop a refined continuum Burton-Cabrera-Frank formalism, which accounts for a lack of equilibration of island shape and importantly also for inhibited incorporation of adatoms at almost-faceted $\langle \bar{1}10 \rangle$ island edges through effective kinetic coefficients. This formalism is shown to describe accurately the adatom diffusion fluxes between islands and thus island evolution for a complex experimental island configuration, as confirmed by matching results from realistic atomistic simulations for this configuration. This approach also elucidates basic dependencies of flux on island geometry and temperature. Second, a further refinement is presented incorporating separate terrace and edge adatom density fields either in a continuum setting or alternatively in a spatially discrete diffusion equation setting. The second approach allows more flexibility and accuracy in accounting for edge-diffusion kinetics including corner rounding, a lack of equilibration of the edge adatom density at $\langle \bar{1}10 \rangle$ island edges, and the effect of rare kinks on $\langle \bar{1}10 \rangle$ island edges. Significantly, it suggests facile two-way corner rounding at the island periphery during island decay, contrasting the previous picture.

PACS number(s): 68.35.Fx, 68.43.Jk, 68.37.Ef, 68.55.−a

I. INTRODUCTION

Submonolayer homoepitaxial films consist of arrays of single-atom-high two-dimensional (2D) islands on perfectly flat terraces of extended single-crystal surfaces. These provide ideal systems for analysis of the details of 2D coarsening processes.[1,2] The most common scenario for coarsening is Ostwald ripening (OR)[3] wherein smaller than average islands shrink, transferring their adatoms by diffusion across terraces to larger islands. Typically, equilibration of island shape is facile during the coarsening process, with individual islands maintaining their equilibrium shape, which is determined according to the Wulff construction by the orientation-dependent step-edge energies for 2D clusters.[4] The thermodynamic driving force for coarsening process derives from the reduction in the energy cost associated with broken bonds at island edges, and this is achieved by decreasing the overall island perimeter length.[5] The preferential dissolution of smaller clusters with higher average edge curvatures reflects their higher chemical potential, a quantity which is well-defined given the assumed equilibrium island shapes.

A basic understanding of island evolution during OR is often provided by a continuum Burton-Cabrera-Franck (BCF)[6] type "step dynamics" formulation.[4,7] This formulation involves analysis of a boundary value problem (BVP) for the diffusion equation describing the density of mobile adatoms on the terraces between islands with appropriate boundary conditions (BCs) at island edges. These BCs account for both the island chemical potentials and for the ease or difficulty of adatom attachment-detachment through so-called kinetic coefficients. It suffices to adopt a steady-state approximation since the adatom density relaxes quickly to the local island

configuration. Solution of this BVP gives net fluxes for attachment-detachment and, thus, island growth or decay rates. Thus, the island configuration can be incrementally updated using these rates, the BVP re-solved to obtain new rates, and the island configuration further evolved, etc. Often instead of analyzing this many-island problem, just the evolution of a single island within a "typical environment" is determined to provide input to the continuity equation for evolution of the island size distribution in a Lifshitz-Slyozov-Wagner theory.[2,5]

The above picture applies to isotropic systems and also to mildly anisotropic systems. However, for strongly anisotropic systems, one might anticipate qualitatively different behavior. The traditional expectation is for a complete absence of deterministic OR in purely one-dimensional (1D) systems where all islands have the same chemical potential.[8] In contrast, coarsening does occur in strongly anisotropic 2D systems. For example, scanning tunneling microscopy (STM) studies by Morgenstern *et al.*[9,10] revealed coarsening for rectangular Ag islands on an Ag(110) surface at a lower temperature (T) of around 220 K or below but via an unusual 1D decay mode. Smaller islands shrank in length while retaining fixed width in the $\langle 001 \rangle$ direction and thus were unequivocally not shape equilibrated.[11,12] Our goal here is to develop appropriate analytical formalisms to describe this 1D decay behavior.

In Sec. II, we provide an atomistic-level description of the thermodynamics and surface diffusion kinetics for submonolayer fcc (110) homoepitaxial systems. Experimental observations for 1D decay of Ag islands on Ag(110) and kinetic Monte Carlo (KMC) simulation results for a realistic atomistic model for this process are also presented. Then, in Sec. III, we refine the standard continuum BCF formulation to treat these strongly anisotropic systems. Refined BCF (rBCF)

predictions for decay rates of islands in strongly anisotropic fcc (110) homoepitaxial systems are presented for canonical local island environments, demonstrating the key dependencies on island geometry and surface temperature. Predictions are then provided for island decay in a complex island distribution taken from STM experiments. Success is confirmed by comparison against realistic atomistic simulations for the same configuration, thereby avoiding uncertainty in direct comparison with experiment due to large intrinsic fluctuations. However, this rBCF approach does not have the flexibility to describe the details of edge diffusion kinetics such as corner or kink rounding and neglects the lack of local equilibration of edge adatoms. Thus, in Sec. IV, we present a further refined formalism with multiple adatom density fields to better capture edge-diffusion kinetics first within a continuum framework and then through an alternative spatially discrete diffusion equation (DDE) formalism.[13] This approach is shown to reduce slight discrepancy seen from comparing the rBCF treatment and realistic atomistic simulation. The approach allows assessment of the effect of rare kinks that act as traps for diffusing atoms on almost-faceted $\langle \bar{1}10 \rangle$ island edges. Most significantly, it suggests facile two-way corner rounding at island edges during island decay, contrasting the previous picture for island decay in this system.[9–11]

II. HOMOEPITAXIAL FCC (110) SURFACE DYNAMICS AND 1D ISLAND DECAY

A. Atomistic models for surface diffusion kinetics

A fcc (110) surface consists of an array of parallel channels (see Fig. 1). The surface unit cell is rectangular with side length b in the $\langle \bar{1}10 \rangle$ direction, $a = \sqrt{2}b$ in the $\langle 001 \rangle$ direction, and area $\Omega = ab$. Adatoms hop between the preferred in-channel adsorption sites (supported by four atoms in the underlying surface layer) through bridge-site transition states (TS). These TS differ for in-channel and cross-channel hopping, as do the diffusion barriers $E_d^{\parallel}$ and $E_d^{\perp}$, respectively. Here, one caveat is

that cross-channel diffusion could instead occur preferentially via exchange for some homoepitaxial fcc (110) systems.

Surface thermodynamics is determined by conventional interactions between adatoms on preferred adsorption sites. We assume nearest-neighbor pairwise attractions with a larger (smaller) magnitude $E_b^{\parallel} < 0$ ($E_b^{\perp} < 0$) for atoms separated by b (a) in the $\langle \bar{1}10 \rangle$ ($\langle 001 \rangle$) direction. For a realistic description of surface-diffusion kinetics, including edge diffusion and detachment, we adopt a multisite lattice-gas (msLG) model[14–16] in which we prescribe a second set of unconventional interactions between one adatom at a TS and others at nearby adsorption sites. Again, just short-range pairwise attractions are assumed [($E_b'^{\parallel} < 0$ and $E_b'^{\perp} < 0$); see Fig. 1]. The total energy, E_i, in the initial state before hopping, and the total TS energy, E_{TS}, can be determined as the sum of the relevant adsorption energy and pairwise interactions; then the activation barrier for hopping is simply determined as $E_{act} = E_{TS} - E_i$ (Refs. 14–16), which equals the sum of isolated adatom diffusion barrier and the difference in total interaction energy between the TS and initial state. This formalism is more flexible than the standard initial value approximation, which sets the unconventional interactions to zero.[17–19] Hop rates are described by an Arrhenius form, $h = \nu e^{-\beta E_{act}}$, with common prefactor $\nu = 10^{13}/\text{s}$ and inverse temperature $\beta \equiv 1/(k_B T)$, where k_B is the Boltzmann constant. For Ag/Ag(110), an appropriate choice of energetics is described in Ref. 11. For this study, the parameters of most importance are $E_d^{\parallel} = 0.28$ eV, $E_d^{\perp} = 0.38$ eV, $E_b^{\parallel} = -0.18$ eV, $E_b^{\perp} = -0.045$ eV, and a $\langle \bar{1}10 \rangle$ to $\langle 001 \rangle$ corner-rounding barrier of $E_{cr} = 0.39$ eV (Ref. 20; see Fig. 1).

The key features proposed to produce 1D island decay for Ag/Ag(110) at lower T described in Sec. I are as follows (Refs. 9 and 11): (i) Detachment of atoms almost exclusively from the short $\langle 001 \rangle$ ends of islands. (ii) A lack of detachment from faceted long $\langle \bar{1}10 \rangle$ sides, and a lack of corner rounding from the $\langle 001 \rangle$ ends to the $\langle \bar{1}10 \rangle$ sides (but see Sec. IV B). (iii) Inhibited nucleation of new layers on the $\langle \bar{1}10 \rangle$ sides, and facile corner rounding of edge atoms from the $\langle \bar{1}10 \rangle$ sides to the $\langle 001 \rangle$ ends. See Fig. 1 for our notation.

B. Key experimental observations for Ag/Ag(110)

The key experimental STM observations for coarsening of rectangular Ag islands on the anisotropic Ag(110) surface, as well as details of the experimental procedures, have been described in Morgenstern *et al.*[9,10] and Han *et al.*[11] Above about 220 K, classic OR behavior is observed with individual islands retaining their equilibrium shapes during growth or decay.[9] If $L^{\parallel}$ ($L^{\perp}$) denotes the length (width) of rectangular islands in the $\langle \bar{1}10 \rangle$ ($\langle 001 \rangle$) direction, then the area satisfies $A \approx L^{\parallel} L^{\perp}$, and the aspect ratio is given by $R \equiv L^{\parallel}/L^{\perp}$. For equilibrated island shapes, one has that $R = R_{eq} \approx 3$ (Ref. 9). However, at 220 K and below, a 1D decay mode is observed: smaller (and narrower) islands shrink in length, $L^{\parallel}$, while retaining constant width, $L^{\perp}$, thus increasing R. This behavior is observed down to about 175 K, at which point the coarsening process becomes too slow to be readily tracked. Analysis of more extensive experimental data indicates that the island decay rate $K = -dA/dt \propto e^{-\beta E_{OR}}$ has an Arrhenius
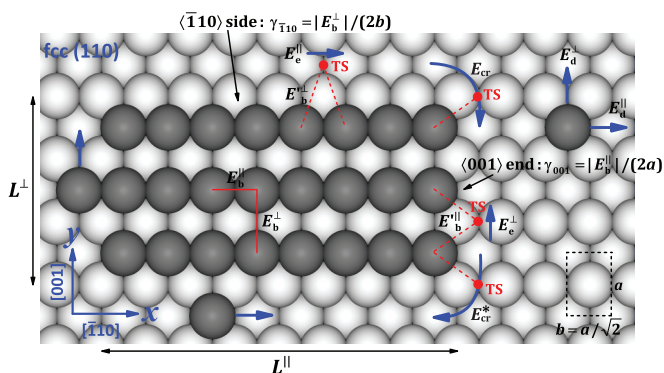
FIG. 1. (Color online) Schematic of a 2D rectangular homoepitaxial island on an fcc (110) surface. Also indicated are anisotropic terrace diffusion barriers ($E_d^{\parallel}$ and $E_d^{\perp}$); conventional pairwise interactions ($E_b^{\parallel}$ and $E_b^{\perp}$) and associated step energies ($\gamma_{\bar{1}10}$ and γ_{001}); unconventional interactions ($E_b'^{\parallel}$ and $E_b'^{\perp}$) for an adatom at a transition state (TS) for edge diffusion; edge-diffusion barriers ($E_e^{\parallel}$ and $E_e^{\perp}$); corner-rounding barriers (E_{cr} and E_{cr}^*); and the surface unit cell as well as notations for island dimensions and in-surface directions.
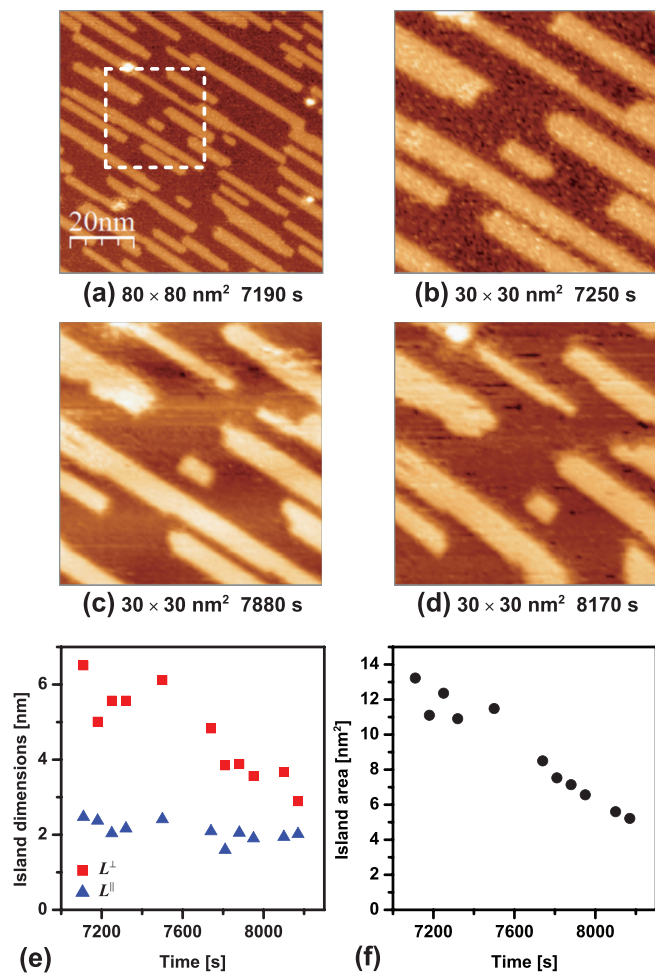
FIG. 2. (Color online) 1D decay of a small rectangular Ag island on Ag(110) at 190 K. (a) Larger scale STM image; (b)–(d) 30×30 nm^2 subregion following decay; (e) island linear dimensions ($L^{\parallel}$ and $L^{\perp}$); and (f) island area versus time (since Ag deposition).

dependence with $E_{OR} \approx 0.32$ eV (Ref. 11). In Fig. 2, we provide an example of this 1D island decay at 190 K, which will be analyzed in detail below.

C. KMC simulation results for 1D island decay on Ag/Ag(110)

Figure 3 shows the results of extensive simulations of the 1D decay process at 190 K for the small island shown in Fig. 2. These simulations were performed using our atomistic msLG model described in Sec. II A. Input to the simulations is the multi-island configuration mimicking the local environment of the decaying island. In addition, we perform atom-tracking KMC simulations labeling adatoms originally in the decaying island with a different color so as to track their transfer to other islands. Given the small island size and low temperature, there are significant fluctuations in the decay process. As a consequence, to reliably assess typical or average behavior, we perform ~100 trials and average the results. From the decrease of the average area of the decaying island, we extract an initial decay rate of $K_{msLG} \approx 0.0026$ nm^2/s. However, after a transient period of ~750 s, there appears to be a slight increase in rate to $K_{msLG} \approx 0.0033$ nm^2/s (measured between ~750 s
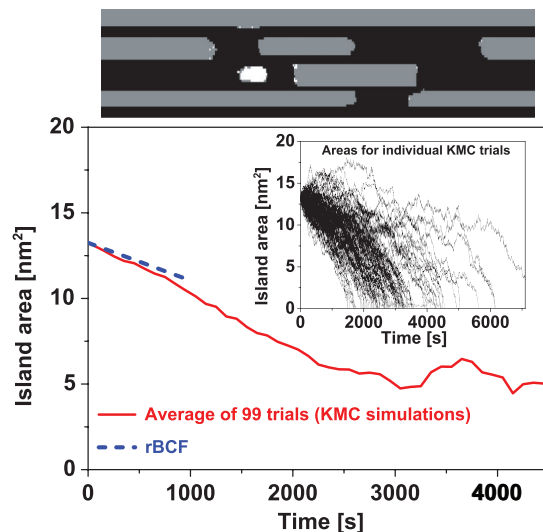
FIG. 3. (Color online) KMC simulation of our atomistic model for decay at 190 K of the Ag island on Ag(110) in Fig. 2. Top frame: Snapshot of the simulated island configuration early during decay. Atoms initially in the decaying island of interest are colored white. Bottom frame: Area versus time averaged over 99 simulation trials. Large noise $t > 2000$ s reflects the limited number of trials with a surviving island. Inset: Areas for individual trials. The dashed blue line indicates the prediction of rBCF theory.

and ~1500 s). The apparent discrepancy between the average msLG rates and the experimental rate $K_{expt} \approx 0.007$ nm^2/s is not unexpected given the very large fluctuations in the results for individual simulation trials.

III. rBCF THEORY FOR ANISOTROPIC SYSTEMS WITHOUT ISLAND EQUILIBRATION

Here, we refine traditional continuum BCF type formulations to better describe coarsening in strongly anisotropic systems and, specifically, 1D island decay with a large deviation from island-shape equilibration. Our focus is on determining for the decay rate, $K_{rBCF} = -dA/dt$, of smaller narrower islands from our rBCF theory.

A. Constrained thermodynamics

For fcc (110) homoepitaxial systems with rectangular islands, the key thermodynamic parameters in our atomistic model are the chemical potential for an infinite island, $\mu_{\infty} = \mu_{ads} + \mu_{int}$ (where μ_{ads} is the isolated adatom adsorption energy, and $\mu_{int} = E_b^{\parallel} + E_b^{\perp}$), and the higher (lower) step energy per unit length, $\gamma_{001} = |E_b^{\parallel}|/(2a)$ ($\gamma_{\bar{1}10} = |E_b^{\perp}|/(2b)$) for steps aligned in the $\langle 001 \rangle$ ($\langle \bar{1}10 \rangle$) direction (see Fig. 1). The energy of an island with linear dimension $L^{\parallel}$ ($L^{\perp}$) in the $\langle \bar{1}10 \rangle$ ($\langle 001 \rangle$) direction and area $A \approx L^{\parallel}L^{\perp}$ can be written as

$$E_{isl} = \frac{A}{\Omega}\mu_{\infty} + (2\gamma_{\bar{1}10}L^{\parallel} + 2\gamma_{001}L^{\perp}). \quad (1)$$

Given the lack of island-shape equilibration, we introduce partial chemical potentials, μ_M, for different possible modes, M, of island evolution.[11,21,22] For this study, the most relevant mode $M = 001$ involves changing length $L^{\parallel}$ with constant width $L^{\perp}$. Then, $\mu_{001} = \Omega dE_{isl}/dA$ obtained using

$dA = L^{\perp}dL^{\parallel}$ with fixed $L^{\perp}$ yields

$$\mu_{001} = \mu_{\infty} + 2\Omega\gamma_{\bar{1}10}/L^{\perp}. \qquad (2)$$

Introducing μ_{001} assumes a degree of local equilibration that should also apply for the dilute ideal 2D adatom gas at the $\langle 001 \rangle$ island edge. If n_{eq} denotes the locally equilibrated adatom gas density per site at the $\langle 001 \rangle$ island edge, then its chemical potential is given by $\mu_{\text{gas}} = \mu_{\text{ads}} + k_{\text{B}}T \ln n_{\text{eq}}$. Since μ_{gas} must match μ_{001}, it follows that n_{eq} equals[11,23]

$$n_{001} = n_{\infty}e^{2\beta\Omega\gamma_{\bar{1}10}/L^{\perp}} \text{ at } \langle 001 \rangle \text{ ends.} \qquad (3)$$

Here, $n_{\infty} = e^{\beta\mu_{\text{int}}}$ denotes the equilibrium adatom density at an extended straight step. Finally, for the observed 1D decay mode $M = 001$, Eqs. (2) and (3) indicate that narrower islands with smaller $L^{\perp}$ and therefore higher μ_{001} and n_{001} should shrink, while wider islands with bigger $L^{\perp}$ and therefore lower μ_{001} and n_{001} grow.

Similarly, defining a mode $M = \bar{1}10$ for changing width $L^{\perp}$ with fixed length $L^{\parallel}$, one has that $\mu_{\bar{1}10} = \mu_{\infty} + 2\Omega\gamma_{001}/L^{\parallel}$ and n_{eq} equals $n_{\bar{1}10} = n_{\infty}e^{2\beta\Omega\gamma_{001}/L^{\parallel}}$ at $\langle \bar{1}10 \rangle$ island edges. Now, for equilibrated island shapes (occurring at higher T), one must have that $\mu_{001} = \mu_{\bar{1}10}$, which yields the equilibrium aspect ratio $R_{\text{eq}} \equiv L_{\text{eq}}^{\parallel}/L_{\text{eq}}^{\perp} = \gamma_{001}/\gamma_{\bar{1}10}$.

B. rBCF formulation for kinetics

Analytic BCF formulations of OR are based on a steady-state analysis of the diffusion equation for the adatom density, n, which for fcc (110) homoepitaxial systems has the form

$$\frac{\partial}{\partial t}n = D^{\parallel}\frac{\partial^2}{\partial x^2}n + D^{\perp}\frac{\partial^2}{\partial y^2}n \approx 0, \qquad (4)$$

where $D^{\parallel} \equiv D_0^{\parallel}e^{-\beta E_d^{\parallel}}$ ($D^{\perp} \equiv D_0^{\perp}e^{-\beta E_d^{\perp}}$) is the larger (smaller) diffusion coefficient in the $\langle \bar{1}10 \rangle$ ($\langle 001 \rangle$) x (y) direction given that $0 < E_d^{\parallel} < E_d^{\perp}$. We assume a common attempt frequency for hopping, ν, so that $D_0^{\parallel} = b^2\nu$ and $D_0^{\perp} = a^2\nu$. Appropriate BCs must be imposed at island edges. The lack of island-shape equilibration is addressed by assigning separate partial chemical potentials and equilibrium adatom densities to the $\langle \bar{1}10 \rangle$ and $\langle 001 \rangle$ edges.

In a general Chernov formulation, the BCs are written as[7]

$$\pm D^{\parallel}\frac{\partial n}{\partial x} = k_{001}(n - n_{001}) \qquad (5a)$$

at $\langle 001 \rangle$ edges, and

$$\pm D^{\perp}\frac{\partial n}{\partial y} = k_{\bar{1}10}(n - n_{\bar{1}10}) \qquad (5b)$$

at $\langle \bar{1}10 \rangle$ edges. The $+(-)$ sign applies for the right (left) edge of the island in Eq. (5a) and the upper (lower) edge in Eq. (5b). In a traditional macroscopic setting,[24] the kinetic coefficients, k_{001} and $k_{\bar{1}10}$, which describe the ease of attachment, would traditionally be taken as $k_{001}^{\text{macro}} = D^{\parallel}/(e^{\beta\delta_{001}} - 1)$ and $k_{\bar{1}10}^{\text{macro}} = D^{\perp}/(e^{\beta\delta_{\bar{1}10}} - 1)$ where δ_{001} and $\delta_{\bar{1}10}$ denote the additional energy barriers for attachment at $\langle 001 \rangle$ and $\langle \bar{1}10 \rangle$ steps, respectively.[13,25] Such barriers are generally zero for homoepitaxial systems, and thus the kinetic coefficients are generally taken as infinite for so-called terrace-diffusion-limited coarsening. Then, Eqs. (5a) and (5b) reduce to simple

Dirichlet BCs: $n = n_{001}$ at $\langle 001 \rangle$ edges, and $n = n_{\bar{1}10}$ at $\langle \bar{1}10 \rangle$ edges, respectively.

Solution of this Dirichlet BVP allows determination of the integrated net-detachment flux for each edge of each island. These determine the rate at which the island dimensions change if one assumes negligible transfer of adatoms by edge diffusion between different island edges. However, even for small $D^{\perp}$, these traditional Dirichlet BCs would lead to a tendency for widening of islands for aspect ratio $R > R_{\text{eq}}$ where $n_{\bar{1}10} < n_{001}$. Likewise, there is a tendency for narrowing when $R < R_{\text{eq}}$ and $n_{001} < n_{\bar{1}10}$. This is not consistent with the 1D decay observed in experiment.

Our resolution to this dilemma is to argue that the traditional macroscale Chernov-type kinetic coefficients in a BCF formulation must be modified for analysis of nanoscale evolution. Specifically, this modification is required when the characteristic length scale of the decaying objects does not greatly exceed the characteristic separation, L_{kink}, between kinks at island edges.[13] The underlying concept is that true attachment at steps requires incorporation at kink sites and is thus inhibited for low kink densities even in the absence of an additional energetic barrier for attachment. This is the case for the smooth almost-faceted $\langle \bar{1}10 \rangle$ island edges. As a result, we introduce a more appropriate very small effective kinetic coefficient, $k_{\bar{1}10} \sim D^{\perp}/L_{\text{kink}}^2$ for attachment to the $\langle \bar{1}10 \rangle$ step edge,[13] which would be negligible for an almost-faceted step edge with large L_{kink}. The kinetic coefficient k_{001} can reasonably be taken as infinite since $\langle 001 \rangle$ steps are highly kinked. Within this formalism incorporating $k_{\bar{1}10} = 0$, one immediately recovers 1D decay.

In closing, we note a previous BCF-type treatment by Yao *et al.*[23] for Ag island decay on Ag(110). They incorporated finite kinetic coefficients $k^{\parallel} \ll k^{\perp}$ based on the inequality $D^{\parallel} \ll D^{\perp}$, although this only follows in the traditional macroscopic theory for nonzero $\delta_{001} \approx \delta_{\bar{1}10}$; however, Yao *et al.* did not discuss the assignment of finite $k^{\parallel}$ and $k^{\perp}$ in the absence of energetic barriers to attachment. They also predicted a different scaling in time for the island decay rate from the behavior which we describe below.

C. rBCF analysis for benchmark island configurations

Islands in experimental distributions are often reasonably well aligned end-to-end with their neighbors in the $\langle \bar{1}10 \rangle$ direction.[11] Thus, we first consider a benchmark configuration with just two aligned islands of differing widths in a rectangular simulation cell with periodic BCs (see Fig. 4). This enables more systematic analysis and elucidation of the fundamental behavior. We set $E_d^{\perp} - E_d^{\parallel} = 0.1$ eV for Ag/Ag(110) and set the temperature to 190 K unless otherwise stated. This implies that $\varepsilon \equiv D^{\perp}/D^{\parallel} = 0.00445$. Below, $L_{\text{cell}}^{\perp}$ will denote the width of the simulation cell and $L_{\text{narrow}}^{\perp}$ ($L_{\text{wide}}^{\perp}$) the width of the narrow (wide) island in the $\langle 001 \rangle$ direction. Corresponding dimensions in the $\langle \bar{1}10 \rangle$ direction are denoted by superscript $\parallel$. If L_{sep} denotes the separation between islands in the $\langle \bar{1}10 \rangle$ direction, then one has $L_{\text{cell}}^{\parallel} = 2L_{\text{sep}} + L_{\text{narrow}}^{\parallel} + L_{\text{wide}}^{\parallel}$. Precise determination of the decay rate, K_{rBCF}, for the narrower island from our rBCF theory and its dependence on various geometric and model parameters is achieved from numerical analysis of the diffusion problem using FEMLAB software.[26]
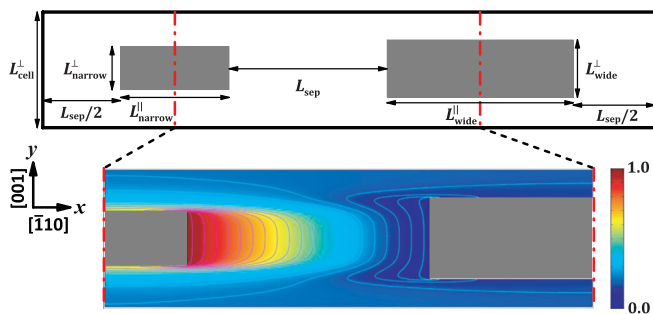
FIG. 4. (Color online) Simulation cell with periodic BCs for a benchmark configuration with a pair of islands aligned end-to-end shown (top row). FEMLAB results for the rescaled adatom density $\delta n^* \equiv (n - n_{001}^{\text{wide}})/(n_{001}^{\text{narrow}} - n_{001}^{\text{wide}})$ in the rBCF problem for the central portion of the cell (bottom row). There are vanishing diffusion fluxes across red dot-dashed lines through island centers. Geometric parameters for the simulated configuration are $R_{\text{narrow}} \equiv \frac{L_{\text{narrow}}^{\parallel}}{L_{\text{narrow}}^{\perp}} = 3$, $\frac{L_{\text{cell}}^{\perp}}{L_{\text{narrow}}^{\perp}} = 2.5$, $\frac{L_{\text{sep}}}{L_{\text{narrow}}^{\parallel}} = 1.5$, $\frac{L_{\text{wide}}^{\parallel}}{L_{\text{narrow}}^{\parallel}} = 2$, and $\frac{L_{\text{wide}}^{\perp}}{L_{\text{narrow}}^{\perp}} = 1.5$.

The bottom frame in Fig. 4 shows results for the rescaled adatom density, $\delta n^* \equiv (n - n_{001}^{\text{wide}})/(n_{001}^{\text{narrow}} - n_{001}^{\text{wide}})$. Thus, δn^* takes values of 1 (0) at the end of the narrower (wider) island. From these results, we can calculate the net detachment fluxes integrated along $\langle 001 \rangle$ island ends after multiplying integrated rescaled fluxes, $\int \frac{\partial}{\partial x} \delta n^* dy$, by $D^{\parallel}(n_{001}^{\text{narrow}} - n_{001}^{\text{wide}})$.

For this aligned island geometry, given the strong anisotropy in terrace diffusion at 190 K, it is natural to assess the effectiveness of a quasi-1D estimate, K_{1D}, of the island decay rate. This estimate corresponds to the diffusion flux in the $\langle \bar{1}10 \rangle$ (x-) direction rate for $D^{\perp} = 0$ (and, therefore, $\varepsilon = 0$) and has the form

$$K_{\text{1D}} = 2D^{\parallel} \frac{L_{\text{narrow}}^{\perp}}{L_{\text{sep}}} \left(n_{001}^{\text{narrow}} - n_{001}^{\text{wide}} \right)$$

$$\approx \frac{4D^{\parallel} n_{\infty} \beta \Omega \gamma_{\bar{1}10}}{L_{\text{sep}}} \left(1 - \frac{L_{\text{narrow}}^{\perp}}{L_{\text{wide}}^{\perp}} \right). \quad (6)$$

The latter expression follows after adopting an approximation for the adatom density $n_{001} = n_{\infty} e^{2\beta\Omega\gamma_{\bar{1}10}/L^{\perp}} \approx n_{\infty} + 2n_{\infty}\beta\Omega\gamma_{\bar{1}10}/L^{\perp}$.

For the geometry in Fig. 4 but varying L_{sep}, we first compare the exact K_{rBCF} with K_{1D}. The agreement is particularly good if the separation, L_{sep}, between the islands is comparable to the island length: $K_{\text{rBCF}}/K_{\text{1D}} = 1.12$, 1.20, 1.27, and 1.31, for $L_{\text{sep}}/L_{\text{narrow}}^{\parallel} = 1$, 2, 4, and 8, respectively. For larger L_{sep}, the agreement degrades for broader simulation cells. A key feature reflecting quasi-1D behavior is the dependence $K_{\text{rBCF}} \sim 1/L_{\text{sep}}$ on L_{sep}, where all other parameters are fixed. This feature is well-satisfied as $L_{\text{sep}} K_{\text{rBCF}}$ increases by only 3%, 6%, 14%, and 17%, as $L_{\text{sep}}/L_{\text{narrow}}^{\parallel}$ increases from 1 to 1.5, 2, 4, and 8, respectively. This inverse proportionality is less well satisfied for broader simulation cells. Such a decrease in K_{rBCF} with increasing L_{sep} is much stronger than the logarithmic dependence found in isotropic systems.[11] This feature impacts the T-dependence of island decay (see Sec. III E). See the Appendix for analysis of the dependence of K_{rBCF} on other model parameters.

Certainly there are examples in experimental island distributions where neighboring islands in the $\langle \bar{1}10 \rangle$ direction are completely misaligned. It is clear that the net flux of diffusing adatoms between such islands (which is mediated by slow cross-channel diffusion) will be relatively small. There are also cases, as shown in Sec. III D, where neighboring islands are marginally misaligned, so that the top $\langle \bar{1}10 \rangle$ edge of one island is aligned with the bottom $\langle \bar{1}10 \rangle$ edge of the neighbor. The net flux between such islands for large anisotropy, $\varepsilon \ll 1$, should be significantly higher than for completely misaligned islands. Separate analysis for the simpler benchmark configurations reflecting these possibilities for misalignment will help elucidate evolution for general arrays of islands. To this end, we take the configuration in Fig. 4 to misalign the islands by shifting in the $\langle 001 \rangle$ direction to achieve marginal (with $L_{\text{cell}}^{\perp} = 2.5 L_{\text{narrow}}^{\perp}$) or complete (with $L_{\text{cell}}^{\perp} = 3 L_{\text{narrow}}^{\perp}$) misalignment. FEMLAB analysis determines the variation of K_{rBCF} with $\varepsilon \to 0$: K_{rBCF} decreases by a factor of 0.54, 0.16, and 0.03 (0.39, 0.06, and 0.005) as ε decreases by a factor of 10, 100, and 100 from $\varepsilon = 0.1$, suggesting that $K_{\text{rBCF}} \sim \varepsilon^{1/2}$ ($K_{\text{rBCF}} \sim \varepsilon^1$), as $\varepsilon \to 0$, for marginally (completely) misaligned islands. These features are clarified in Sec. III E.

D. rBCF analysis for an experimental island configuration

For configurations of multiple islands, including those extracted from experimental STM images, it is also viable to solve the multi-island rBCF BVP numerically using FEMLAB software. In this way, one can compare rBCF predictions for island evolution and particularly the 1D decay of narrower islands, with experimental observations or with corresponding KMC simulations. To this end, we input to our numerical analysis a configuration of several islands shown in Fig. 5 (top) that constitute the local environment of the narrow decaying island tracked in Fig. 2. We choose the boundary of the simulation region to correspond roughly to a physical zero-flux boundary. Note, however, that the specific treatment
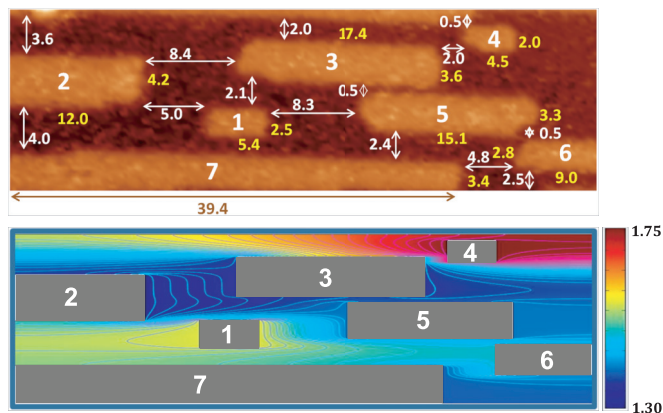
FIG. 5. (Color online) Top: Magnified STM image (50.0 × 15.5 nm²) for the local environment of the small narrow decaying island shown in Fig. 2. Island dimensions are shown in yellow and separations in white (in nm). Bottom: FEMLAB results for the rescaled adatom density field, $n^{\dagger} \equiv n/n_{\infty}$, in the rBCF treatment for the island configuration (top). The simulation cell has zero-flux BCs at the outer edges.

of the outer boundary will not greatly affect the evolution of the far-removed small, narrow central island. For each of the islands, we impose a zero-flux BC on the top and bottom $\langle \bar{1}10 \rangle$ edges and a suitable Dirichlet BC on the $\langle 001 \rangle$ ends. From Eq. (3), the latter BC sets the adatom densities, n, to

$$n_{001} = n_\infty e^{2\beta\Omega\gamma_{\bar{1}10}/L^\perp} = n_\infty e^{\beta a |E_b^\perp|/L^\perp} \approx n_\infty e^{1.124/L^\perp} \quad (7)$$

at 190 K, with $|E_b^\perp| = 0.045$ eV for Ag/Ag(110) (Ref. 11) and with $L^\perp$ in nm.

Results of our FEMLAB analysis for the rescaled density field $n^\dagger = n/n_\infty$ are shown in Fig. 5 (bottom). From these results, we can calculate the net detachment fluxes integrated along $\langle 001 \rangle$ ends of any island[27] after multiplying integrated rescaled fluxes $\int \frac{\partial}{\partial x} n^\dagger dy$ by $D^\parallel n_\infty = 0.0336$ nm^2/s at 190 K using parameters for Ag/Ag(100) in Ref. 11. The calculated net detachment rate from the right side of the small central island 1 is $K_{\text{rBCF,1R}} = 0.00147$ nm^2/s and from the left side is $K_{\text{rBCF,1L}} = 0.00073$ nm^2/s. Thus, the total rate of decay of the area of island 1 is $K_{\text{rBCF,1}} = 0.0022$ nm^2/s.

It is natural to compare the value of $K_{\text{rBCF,1R}}$ with a simple 1D estimate. We note that a segment of length $L'^\perp = 1.7$ nm on the right end of island 1 (with $L_1^\perp = 2.5$ nm) is directly aligned with the left end of island 5 to the right (with $L_5^\perp = 3.3$ nm), which is separated from island 1 by a distance $L_{\text{sep}}^{1\rightarrow5} = 8.3$ nm. Thus, it follows that

$$K_{\text{1D,1R}} = D^\parallel n_\infty (e^{1.124/L_1^\perp} - e^{1.124/L_5^\perp})$$
$$\times L'^\perp / L_{\text{sep}}^{1\rightarrow5} = 0.0011 \text{ nm}^2/\text{s},$$

which just 25% below $K_{\text{rBCF,1R}}$. The left end of island 1 is misaligned with the neighboring island to the left, but just marginally, so that $K_{\text{rBCF,1L}}$ is still significant relative to $K_{\text{rBCF,1R}}$. Both features can be anticipated from the results in Sec. III C.

There are complications in direct comparison of rBCF results with the experimental observations in Sec. II B. Most significantly, island decay is highly stochastic for smaller islands at 190 K (cf. Sec. II), so experimentally observed behavior may not be typical. Indeed, the experimental decay rate $K_{\text{expt,1}}$ (of perhaps 0.005 nm^2/s initially, increasing to $\approx$0.007 nm^2/s) matches the group of faster decaying trajectories in our KMC simulation study but not the average behavior. Also, the actual shapes of islands neighboring decaying island 1 are not perfect rectangles or even rectangles with rounded corners. Deviations from straight $\langle \bar{1}10 \rangle$ sides imply many more traps for diffusing adatoms than for more perfect islands such as those in our rBCF analysis. This feature might boost decay.

Thus, we instead compare the rBCF results with those from KMC simulation of our msLG model in Sec. II C for the experimental island configuration, thereby gaining two major advantages. First, by repeating the simulation many times for the same initial configuration of island 1 and its local environment, we can obtain precise results for the mean decay rate, i.e., the quantity assessed by rBCF. Second, we can choose the initial shapes of the islands to match the perfect rectangular rBCF shapes rather than including the experimental imperfections. Comparing the initial decay rate for island 1 from our msLG model averaging over 99 trials

(see Sec. II C) with the rBCF result yields good agreement:

$$K_{\text{msLG,1}} = 0.0026 \text{ nm}^2/\text{s} \text{ versus } K_{\text{rBCF,1}} = 0.00219 \text{ nm}^2/\text{s},$$

(see also Fig. 3). Thus, we conclude that the rBCF approach captures the key features of the 1D decay of island 1. Furthermore, it elucidates the details of mass flow between islands in a way that is not possible from experiment and difficult even in KMC simulation.

For BCF-type modeling of island evolution, it is generally necessary to incrementally evolve the island configuration using the initial growth or decay rates, re-solve the BVP, and incrementally evolve islands again, etc. However, for this system, one expects that the island decay rate is roughly constant, so linear decay of the island area is completely determined by initial decay rate (and the initial size). This picture is suggested by either the experimental or KMC data and from the structure of our rBCF theory (decay with fixed island width implies fixed partial chemical potential differences that drive evolution). However, to confirm this expectation, we re-solve the BVP at a later time, where island 1 has decayed to half its initial area, and re-evaluate its decay rate. In the evolved configuration, the right (left) end of island 1 has receded by 1.8 (0.9) nm, so its length has decreased from 5.4 to 2.7 nm. However, the right (left) end of island 2 (island 5) has advanced by 1.2 (1.1) nm so the end-to-end separations between island 1 and its neighbors (which impact the decay rate) do not change much. Also, island 4 has disappeared in the evolved configuration, but this has negligible effect on the decay of island 1. Indeed, the recalculated decay rate $K_{\text{rBCF,1}} = 0.00220$ nm^2/s is very close to the initial value of 0.00219 nm^2/s.

E. Further discussion of the rBCF analysis

Our rBCF analysis has effectively characterized the dependence of the island decay rate on geometry. An additional observation further elucidates this behavior: expanding the y axis by a (large) factor of $r \equiv \varepsilon^{-1/2} \equiv (D^\parallel/D^\perp)^{1/2} = (b/a)e^{\beta(E_d^\perp - E_d^\parallel)/2}$ converts the BVP into one with isotropic diffusion. Since $r = e^{0.05\beta}/\sqrt{2} \approx 15.0$ (here and later, β is always in eV^{-1}) is large for Ag/Ag(110) at 190 K, our benchmark geometry with two aligned islands in the simulation cell transforms into a geometry with two closely spaced wide islands with long parallel nearby edges. Thus, one naturally expects quasi-1D behavior. To obtain the island decay rate, K_{rBCF}, for misaligned islands, one solves for rate, K_{iso}, in the rescaled isotropic problem, and then multiplies by $1/r$, accounting for expanded $\langle 001 \rangle$ island edge lengths. For the marginally misaligned case, clearly K_{iso} achieves a finite-limiting value as $r \rightarrow \infty$, and thus $K_{\text{rBCF}} \sim K_{\text{iso}}/r \sim \varepsilon^{1/2}$, as $\varepsilon \rightarrow \infty$. For the completely misaligned case, one finds that $K_{\text{iso}} \sim 1/r$, so that $K_{\text{rBCF}} \sim 1/r^2 \sim \varepsilon$, as $\varepsilon \rightarrow 0$. This explains the behavior described in Sec. III C.

The rBCF formalism also elucidates basic dependencies of the decay rate, K_{rBCF}, on time and temperature. The form of K_{1D} indicates that K_{rBCF} should be roughly constant, so that the island area, A, should decay linearly, consistent with experiment and simulation in Sec. II. However, previous studies proposed that $A \sim (t_0 - t)^p$, where t_0 is the time of island disappearance, disagreeing on whether $p = 2/3$ (Ref. 9)

or 1/2 (Ref. 23). In either case, since $p < 1$, it follows that $K \sim A^{-(1-p)/p}$ diverges as $A \to 0$. However, these fits were applied to both to the 1D decay regime and a subsequent 2D late-stage regime which occurs for $R < R_{\min} \sim 1$ (Ref. 11). The 2D regime has $p = 2/3$ for terrace-diffusion-limited coarsening in isotropic systems.[11] Thus, their analysis was skewed by also fitting the latter regime.

Finally, we consider the effective Arrhenius energy $E_{OR} = -\frac{d}{d\beta}\ln K$ for 1D island decay at lower T versus conventional 2D decay at higher T. We assign an Arrhenius dependence, $L_{sep} \sim e^{-\beta E_{sep}}$, for the typical distance between $\langle 001 \rangle$ island ends with measured $E_{sep} \approx 0.20$ eV,[11] and write $E_{form} = -\mu_{int} > 0$ for the energy cost to form a 2D gas adatom by extraction of an adatom from a large 2D island. Since, roughly speaking, $K_{1D} \sim D^{\parallel} n_{\infty} / L_{sep}$ for 1D decay versus $K_{2D} \sim (D^{\parallel} D^{\perp})^{1/2} n_{\infty} / \ln L_{sep}$ for 2D decay,[11,23] it then follows that

$$E_{OR,1D} = E_d^{\parallel} + E_{form} - E_{sep} = 0.31 \text{ eV} \quad \text{versus}$$

$$E_{OR,2D} = (E_d^{\parallel} + E_d^{\perp})/2 + E_{form} = 0.56 \text{ eV}.$$

This low $E_{OR,1D}$ matches experiment $E_{expt} \approx 0.32$ eV (Ref. 11) in marked contrast to $E_{OR,2D}$.

IV. MULTIDENSITY FIELD AND SPATIALLY DISCRETE ANALYTIC FORMALISMS

A more detailed analytic treatment of 1D island decay might incorporate a description of edge-diffusion kinetics into the modeling. In Sec. IV A, we suggest formalism still within a continuum BCF-type framework but which includes an additional diffusion field for edge adatoms. However, in any system with nanoscale island dimensions of $\mathcal{O}(10^1)$ lattice constants, one could argue that it is also appropriate to retain spatial discreteness. Then, BCF-type diffusion equations are replaced by so-called lattice differential (diffusion) equations. In fact, such a discrete framework is extremely versatile being amenable to including details of edge-diffusion kinetics as well as other features of nanoscale geometry.[13] This approach is developed in Sec. IV B, and results are presented in Sec. IV C.

A. Analytic continuum formalism

To account for the lack of equilibration of edge adatoms at $\langle \bar{1}10 \rangle$ step edges and to capture the details of edge diffusion kinetics, we introduce a separate diffusion field, n_{edge}, to describe the density per site of edge adatoms at the $\langle \bar{1}10 \rangle$ edges (in addition to the adatom density, n, on terraces). See Refs. 28–30 for somewhat related formalisms. The terrace adatom density, n, satisfies the BCF diffusion equation [Eq. (4)] together with a Dirichlet BC, $n = n_{001}$, at $\langle 001 \rangle$ islands ends (as in Sec. III) and now another Dirichlet BC, $n = e^{\beta E_b^{\perp}} n_{edge}$, on $\langle \bar{1}10 \rangle$ island edges. The latter condition reflects the feature that n_{edge} is enhanced relative to the nearby adatom density on terraces due to bonding to the step edge with strength determined by $E_b^{\perp} < 0$.

Let $J_y(x) = \pm a^{-1} D^{\perp} \frac{\partial}{\partial y} n$ denote the net flux of terrace adatoms per unit length attaching at position x along the $\langle \bar{1}10 \rangle$ edge of an island, where the $+(-)$ sign applies for the lower

(upper) $\langle \bar{1}10 \rangle$ edge. Then, it follows that

$$\frac{\partial}{\partial t} n_{edge} = D_e^{\parallel} \frac{\partial^2}{\partial x^2} n_{edge} + J_y(x) \approx 0, \quad (8)$$

where $D_e^{\parallel} \equiv b^2 h_e^{\parallel}$ is the edge-diffusion coefficient with $h_e^{\parallel} \equiv \nu e^{-\beta E_e^{\parallel}}$. To specify BCs at the corners of the island, we introduce an effective rate, $h_{cr} \equiv \nu e^{-\beta E_{cr}}$ (see Fig. 1) for corner rounding from $\langle \bar{1}10 \rangle$ to $\langle 001 \rangle$ edges. The effective rate for corner rounding in the reverse direction is determined by detailed balance. Then, by matching edge-diffusion flux and the net corner-rounding flux, J_{cr}, from $\langle \bar{1}10 \rangle$ to $\langle 001 \rangle$ edges, this BC becomes

$$D_e^{\parallel} \frac{\partial}{\partial x} n_{edge} = \pm J_{cr} = \pm b h_{cr}\left(n_{edge} - e^{-\beta E_b^{\perp}} n_{001}\right), \quad (9)$$

where the $+(-)$ sign applies for left (right) island corners. The first (second) term on the right-hand side corresponds to corner rounding from $\langle \bar{1}10 \rangle$ to $\langle 001 \rangle$ edges (from $\langle 001 \rangle$ to $\langle \bar{1}10 \rangle$ edges). The extra factor of $e^{-\beta E_b^{\perp}}$ in the negative contribution to J_{cr} ensures that for a single island, the equilibrated $\langle \bar{1}10 \rangle$ edge density satisfies $n_{edge} = e^{-\beta E_b^{\perp}} n_{001}$, i.e., n_{edge} is enhanced relative to n_{001}, which also corresponds to the local adatom density on terraces consistent with the above Dirichlet BC for n at $\langle \bar{1}10 \rangle$ step edges. Further detailed analysis is possible,[31] but here we instead focus on an alternative discrete formalism.

B. DDE formalism

To develop and illustrate the DDE formalism, we first consider the benchmark geometry of two aligned islands in a simulation cell with periodic BCs as in Sec. III C. This geometry and the labeling of a spatially discrete grid of adsorption sites (i, j) is shown in Fig. 6(a). The adatom density at site (i, j) is denoted by $n_{i,j}$. The generic equation for the adatom densities, $n_{i,j}$, has the form

$$\frac{d}{dt} n_{i,j} = h_{i+1,j}^{<} n_{i+1,j} + h_{i-1,j}^{>} n_{i-1,j} + h_{i,j+1}^{\vee} n_{i,j+1}$$
$$+ h_{i,j-1}^{\wedge} n_{i,j-1} - (h_{i,j}^{<} + h_{i,j}^{>} + h_{i,j}^{\vee} + h_{i,j}^{\wedge}) n_{i,j}, \quad (10)$$

where $h_{i,j}^{<}$, $h_{i,j}^{>}$, $h_{i,j}^{\vee}$, and $h_{i,j}^{\wedge}$ denote the rates to hop left, right, down, or up from site (i, j), respectively. The specific form of these rates and the BCs differs for various classes of adsorption sites as enumerated below. Figures 6(a) and 6(b) illustrate these six classes (corner, $\langle \bar{1}10 \rangle$ edge, $\langle 001 \rangle$ edge, boundary, kink, and terrace sites) using six different symbols (diamonds, triangles, dots, squares, stars, and crosses, respectively).

First, we discuss the rates. For the terrace sites not adjacent to $\langle \bar{1}10 \rangle$ edge sites, one has that $h_{i,j}^{<} = h_{i,j}^{>} = h^{\parallel} \equiv \nu e^{-\beta E_d^{\parallel}}$ and $h_{i,j}^{\vee} = h_{i,j}^{\wedge} = h^{\perp} \equiv \nu e^{-\beta E_d^{\perp}}$. For $\langle \bar{1}10 \rangle$ edge sites, a distinct edge-diffusion rate is applied, i.e., $h_{i,j}^{<} = h_{i,j}^{>} = h_e^{\parallel} \equiv \nu e^{-\beta E_e^{\parallel}}$ (Ref. 19). Also, the rate to hop from such sites to near-edge terrace sites is reduced by a factor of $e^{\beta E_b^{\perp}}$ relative to $h^{\perp}$, e.g., for upper $\langle \bar{1}10 \rangle$ edges, one has that $h_{i,j}^{\wedge} = e^{\beta E_b^{\perp}} h^{\perp}$ and $h_{i,j}^{\vee} = 0$. For the corner sites just above or below the $\langle 001 \rangle$ edges, the rate to hop to the $\langle \bar{1}10 \rangle$ edge site is $h_e^{\parallel}$. Rates to hop from such sites to near-edge terrace sites are reduced by a factor of $e^{\beta E_b^{\perp}}$. To capture corner-rounding diffusion kinetics,

the rate to hop from corner to $\langle 001 \rangle$ edge sites is taken as $h_{cr} \equiv \nu e^{-\beta E_{cr}}$, where $E_{cr} = 0.39$ eV (see Fig. 1) consistent with Sec. II A. Thus, for the upper right corner site, one has $h_{i,j}^< = h_e^\parallel$, $h_{i,j}^\wedge = e^{\beta E_b^\perp} h^\perp$, $h_{i,j}^> = e^{\beta E_b^\perp} h^\parallel$, and $h_{i,j}^\vee = h_{cr}$. For sites at $\langle 001 \rangle$ island edges, we impose a Dirichlet BC, $n_{i,j} = n_{001}$, where n_{001} is determined for the appropriate island width and thus is higher for the left island than the right island.[32] Consistently, the rate to hop left or right to an adjacent terrace site is taken as $h^\parallel$. The rate to hop from the top or bottom of the $\langle 001 \rangle$ edges to the corner sites is taken as $c_r e^{-\beta E_b^\perp} h_{cr}$. Choosing $c_r = 1$ satisfies detailed balance and ensures that the equilibrium $\langle \bar{1}10 \rangle$ edge density is enhanced by a factor of $e^{-\beta E_b^\perp}$ relative to the equilibrium terrace density. (Setting $c_r = 0$ artificially enforces one-way corner rounding.) For sites adjacent to boundaries across which there is no diffusion flux (e.g., outer boundaries of the simulation cell), we set to zero the rates for hops which would cross those boundaries.

For all sites in the middle of terraces, Eq. (10) has a generic form. Of course, the form of Eq. (10) differs for edge and corner sites. However, the form of Eq. (10) also differs for near-edge sites adjacent to those at $\langle \bar{1}10 \rangle$ edges due to the modified form of gain terms associated with detachment from $\langle \bar{1}10 \rangle$ edges. This feature and the desire to elucidate the solutions of Eq. (10) motivates a natural rescaling, where we set $n_{i,j}^* = n_{i,j}$ for all terrace sites and $n_{i,j}^* = e^{\beta E_b^\perp} n_{i,j}$ for $\langle \bar{1}10 \rangle$ edge sites. Then, for all terrace sites including those adjacent to $\langle \bar{1}10 \rangle$ edges (but not for $\langle \bar{1}10 \rangle$ edge sites), Eq. (10) adopts the generic form

$$\frac{d}{dt} n_{i,j}^* = h^\parallel (n_{i+1,j}^* - 2n_{i,j}^* + n_{i-1,j}^*)$$
$$+ h^\perp (n_{i,j+1}^* - 2n_{i,j}^* + n_{i,j-1}^*). \quad (11)$$

For the edge of the simulation cell, terms corresponding to crossing the boundary are removed. For most $\langle \bar{1}10 \rangle$ edge sites, one has that

$$\frac{d}{dt} n_{i,j}^* = h_e^\parallel (n_{i+1,j}^* - 2n_{i,j}^* + n_{i-1,j}^*)$$
$$+ e^{\beta E_b^\perp} h^\perp (n_{i,j\pm 1}^* - n_{i,j}^*), \quad (12)$$

where the $+(-)$ applies for the upper (lower) $\langle \bar{1}10 \rangle$ edge. For the corner sites just above the right $\langle 001 \rangle$ island end, one has the special equation

$$\frac{d}{dt} n_{i,j}^* = h_e^\parallel (n_{i-1,j}^* - n_{i,j}^*) + e^{\beta E_b^\perp} h^\parallel (n_{i+1,j}^* - n_{i,j}^*)$$
$$+ e^{\beta E_b^\perp} h^\perp (n_{i,j+1}^* - n_{i,j}^*) + h_{cr}^\perp (c_r n_{i,j-1}^* - n_{i,j}^*). \quad (13)$$

An analogous equation applies for edge sites just below the right $\langle 001 \rangle$ island end, as well as just above and below the left $\langle 001 \rangle$ end.

Each term in Eqs. (11)–(13) with $c_r = 1$ just involves a difference between rescaled densities at adjacent sites. Thus, if both islands have the same width (and n_{001}), one clearly recovers the correct equilibrium solution $n_{i,j}^* = n_{001}$, for all sites. Below we use the further rescaled density $n_{i,j}^\dagger \equiv n_{i,j}^*/n_\infty$ (cf. Sec. III E). Then, the BC at the end of an island of width $L^\perp = \delta j a$ is simply $n_{001}^\dagger = e^{\beta a |E_b^\perp|/L^\perp} \approx e^{2.748/\delta j}$ for Ag/Ag(110) at 190 K with $E_b^\perp = -0.045$ eV.
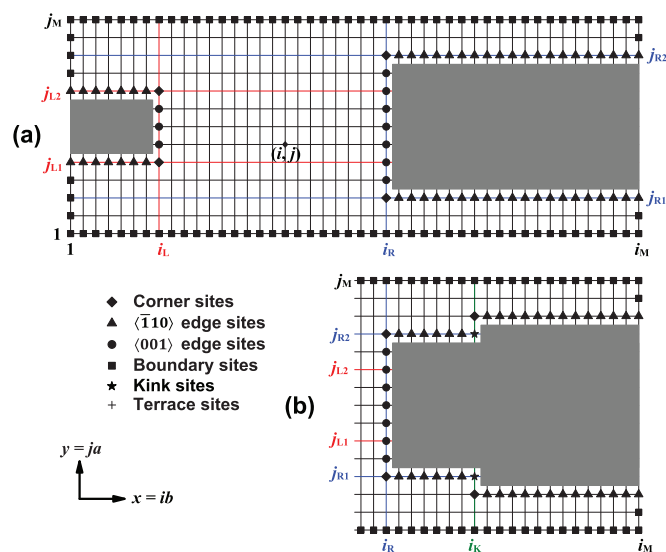
FIG. 6. (Color online) (a) Benchmark-aligned island geometry for the DDE formalism. The region shown corresponds to the central part of Fig. 4 (top) or all of Fig. 4 (bottom). Different types of sites described in the text are indicated by different symbols. (b) Refined geometry for the wider island including kinks. Most results are presented for the choice of geometric parameters: $i_M = 73$, $j_M = 18$ (simulation cell); $i_L = 13$, $j_{L1} = 6$, $j_{L2} = 13$ (narrow island); $i_R = 54$, $j_{R1} = 4$, $j_{R2} = 15$ (wide island); $i_K = 59$.

C. DDE results for benchmark and refined island configurations

We first assess 1D decay for the aligned island configuration shown in Fig. 6 with energetic parameters for Ag/Ag(110) at 190 K (and $c_r = 1$) and geometric parameters $L_{narrow}^\perp \approx 2.5$ nm, $L_{narrow}^\parallel \approx 6.9$ nm for the narrow island ($\delta j = 6$ so $n_{001,narrow}^\dagger = 1.581$), $L_{wide}^\perp \approx 4.1$ nm and $L_{wide}^\parallel \approx 11.0$ nm for the wide island ($\delta j = 10$ so $n_{001,wide}^\dagger = 1.316$), and $L_{sep} \approx 12.1$ nm. Of particular interest is the diffusion flux between islands, $K_{DDE} = -h^\parallel n_\infty (\sum_j n_{i+1,j}^\dagger - n_{i,j}^\dagger) = 0.0504\, h^\parallel n_\infty$, and the net corner-rounding flux is from $\langle \bar{1}10 \rangle$ to $\langle 001 \rangle$ edges, $J_{cr} = h_{cr} n_\infty e^{-\beta E_b^\perp} (n_{corner,narrow}^\dagger - n_{001,narrow}^\dagger)$. The rescaled adatom density $n_{corner,narrow}^\dagger = 1.441$ at corner sites is below $n_{001,narrow}^\dagger = 1.581$, so $J_{cr} < 0$. Thus, our key observation is that there is a small net corner-rounding flux actually from $\langle 001 \rangle$ to $\langle \bar{1}10 \rangle$ edges with $J_{cr}/K_{DDE} = -0.052$. As an aside, J_{cr} is positive for the wider island.

This result presents a fundamentally different picture from that suggested previously (Ref. 9) of effective one-way corner rounding from $\langle \bar{1}10 \rangle$ to $\langle 001 \rangle$ edges with a significant positive corner-rounding flux, $J_{cr} > 0$, for the narrow decaying island. It was argued that such a flux could inhibit the overall 1D decay of the island by feeding detached adatoms back to the $\langle 001 \rangle$ end.[33] However, examination of the BVP for our rescaled equations for the physical choice of $c_r = 1$ makes it clear that the rescaled densities at all sites on the surface, including those at corners, $n_{corner,narrow}^\dagger$, cannot exceed the maximum value of $n_{001,narrow}^\dagger$ for the narrower island. Thus, one must always have $J_{cr} < 0$ for the narrower island during coarsening. In an equilibrium situation corresponding to two equal width islands, there is a balance in the corner-rounding flux in both directions so

$J_{cr} = 0$. In contrast, deposition can create a net flux from $\langle \bar{1}10\rangle$ to $\langle 001\rangle$ edges in narrow islands, $J_{cr} > 0$. In fact, such a flux is responsible for highly elongated growth shapes.[34]

Another key comparison follows from adjusting the model parameters to mimic the rBCF treatment, which does not incorporate binding to $\langle \bar{1}10\rangle$ edges and which does not explicitly treat corner rounding. To this end, we simply set $E_b^\perp = 0$, $h^\parallel = h_e^\parallel$ and also set $h_{cr} = 0$ to capture the feature of no direct corner rounding.[35] We find that $K_{DDE} = 0.0466\, h^\parallel n_\infty$ is somewhat reduced by a factor of 0.92 relative to our above model with realistic treatment of edge diffusion for Ag/Ag(110) at 190 K. This reduction is consistent with the observation in Sec. III that the rBCF prediction for the rate of decay of the island in Fig. 2(a) is slightly below the value obtained from KMC simulation. A more realistic treatment of edge diffusion would improve the agreement with KMC results.

Finally, we further highlight the versatility of the DDE formalism in capturing various features of nanoscale island geometry. Naturally, we can treat marginally or completely misaligned islands, and find the expected decrease in K_{DDE} relative to aligned islands.[36] More significantly, we can add kinks on the $\langle \bar{1}10\rangle$ edges of the wider island [see Fig. 6(b)] to assess the influence of these strong localized trap sites on enhancing the decay of the narrow island. Strong trapping is reflected in the assignment $n_{kink}^\dagger \equiv n_{kink}/n_\infty = 1$, which is below the value of $n_{001}^\dagger = e^{\beta |E_b^\perp|/\delta j}$ at the $\langle 001\rangle$ end of either island. Our analysis retains the geometric parameters used above for aligned islands but adds a single kink at $i_K = 59$ on each $\langle \bar{1}10\rangle$ edge of the wide island. Again with parameters for Ag/Ag(110) at 190 K and $c_r = 1$, we find that $K_{DDE} = 0.0554\, h^\parallel n_\infty$ has increased somewhat above the value of that $K_{DDE} = 0.0504\, h^\parallel n_\infty$ for the corresponding geometry without kink sites. This is also consistent with the slight discrepancy between rBCF and KMC results in Sec. III, noting that kinks at island edges can form spontaneously in the KMC simulations.

V. CONCLUSIONS

Our rBCF modeling in Sec. III accounts for unequilibrated island shapes in contrast to traditional BCF-based theory of coarsening by OR. Importantly, it also accounts for inhibited incorporation of adatoms at almost-faceted $\langle \bar{1}10\rangle$ island edges through the introduction of (small) effective kinetic coefficients, which are relevant for the treatment of nanoscale (versus macroscale) evolution. The rBCF theory provides a predictive modeling tool that captures and elucidates the basic features of 1D decay of islands in strongly anisotropic fcc (110) homoepitaxial systems. This includes description of the unusual dependence of island decay rate on both island geometry and temperature. In particular, rBCF modeling obtains good agreement with precise results for the decay rates obtained from KMC simulations of experimentally observed 1D decay of Ag islands on Ag(110) homoepitaxial at 190 K. It further provides a complete picture of mass flow across the surface during coarsening, e.g., quantifying the relative magnitude of the flux between aligned versus misaligned islands in the experimental system.

However, rBCF theory assumes equilibration of edge adatoms and does not explicitly incorporate edge-diffusion kinetics, the details of which have some influence on the decay rate. Our DDE treatment in Sec. IV accounts for these features and produces a slight enhancement of the island decay rates relative to rBCF theory. The DDE formalism also has the flexibility to allow incorporation of kinks on the $\langle \bar{1}10\rangle$ island edges (contrasting the perfect rectangular islands in the rBCF treatment). Incorporating kinks on the wider islands also slightly enhances the island-decay rate of narrower islands. Both effects improve the already good agreement of the predictions of analytic theory with KMC simulation. A significant feature of the DDE formalism is that it provides a precise characterization of the adatom density along $\langle \bar{1}10\rangle$ edges and associated mass flow around the island periphery. This is not viable in KMC simulations due to fluctuations in low edge densities. We find significant two-way mass flow around corners contrasting the previous picture of flow primarily from $\langle \bar{1}10\rangle$ to $\langle 001\rangle$ edges.[9–11]

Finally, we remark that 1D island decay phenomenon and the type of formalisms developed here should have more general applicability. They apply to other fcc (110) homoepitaxial systems but also to heteroepitaxial systems with strong anisotropy producing elongated islands with almost-faceted long edges (e.g., Ag on NiAl(110)).[37]

APPENDIX: rBCF ANALYSIS FOR BENCHMARK-ALIGNED ISLAND GEOMETRY

Here, we assess the dependence of K_{rBCF} on various other model parameters. First, recall the feature that the thermodynamic driving force for island decay derives from the differences in island width. Thus, it is natural to analyze the change in K_{rBCF} upon varying $L_{wide}^\perp$. For the geometry in Fig. 4 but varying $L_{wide}^\perp$ (setting $L_{cell}^\perp = L_{wide}^\perp + L_{narrow}^\perp$), we find that $K_{rBCF} \approx c\,\delta n_{001}$ with $\delta n_{001} \equiv n_{001}^{narrow} - n_{001}^{wide}$ and where the prefactor c only varies by a few percent. Thus, the enhanced decay rate for wider neighboring islands primarily results from the increased thermodynamic driving force. Second, consistent with the quasi-1D estimate, we find a negligible dependence of K_{rBCF} on the length, $L_{wide}^\parallel$. Third, we explore how the dependence of K_{rBCF} on L_{sep} varies with the degree of anisotropy ε in terrace diffusion. For the benchmark geometry in Fig. 4, we find that the dependence, $K_{rBCF} \sim 1/L_{sep}$, does not degrade upon increasing ε from 0.00445 to 0.0102 [i.e., increasing T from 190 K to 220 K for Ag/Ag(110)] to $\varepsilon = 1$ (isotropic diffusion). The key point is that quasi-1D behavior is induced not just by small ε, but also by the "quasi-1D channel" geometry in which we solve BVP for the diffusion equation. This feature of our benchmark geometry for larger L_{sep} reflects experimental geometries given the presence of highly elongated large islands formed during deposition which form quasi-1D channels[11] (see Fig. 2).

*yong@ameslab.gov

†Current address: Electrochemistry Branch, Power and Energy Division, Sensor and Electron Devices Directorate, U.S. Army Research Laboratory, Adelphi, Maryland 20783, USA.

[1] K. Morgenstern, Phys. Status Solidi B **242**, 773 (2005).

[2] P. A. Thiel, M. Shen, D.-J. Liu, and J. W. Evans, J. Phys. Chem. C **113**, 5047 (2009).

[3] W. Ostwald, *Lehrbuch der Allgemeinen Chemie* (Verlag von W. Engelmann, Leipzig, Germany, 1887), Vol. 2, Part 1.

[4] M. Giesen, Prog. Surf. Sci. **68**, 1 (2001).

[5] L. Ratke and P. W. Voorhees, *Growth and Coarsening: Ripening in Materials Processing* (Springer, Berlin, 2001).

[6] W. K. Burton, N. Cabrera, and F. C. Frank, Philos. Trans. R. Soc. London A **243**, 299 (1951).

[7] H.-C. Jeong and E. D. Williams, Surf. Sci. Rep. **34**, 171 (1999).

[8] L. D. Landau and E. M. Lifshitz, *Course on Theoretical Physics: Statistical Physics* (Permagon, New York, 1959), Vol. 5, p. 482.

[9] K. Morgenstern, E. Lægsgaard, I. Stensgaard, and F. Besenbacher, Phys. Rev. Lett. **83**, 1613 (1999).

[10] K. Morgenstern, E. Lægsgaard, I. Stensgaard, F. Besenbacher, M. Böhringer, W.-D. Schneider, R. Berndt, F. Mauri, A. De Vita, and R. Car, Appl. Phys. A **69**, 559 (1999).

[11] Y. Han, S. M. Russell, A. R. Layson, H. Walen, C. D. Yuen, P. A. Thiel, and J. W. Evans, Phys. Rev. B **87**, 155420 (2013).

[12] Eventually, when the island aspect ratio becomes small enough around $R = R_{min} \approx 1$, there is a transition to 2D decay before island disappearance (Ref. 11).

[13] D. M. Ackerman and J. W. Evans, Multiscale Model. Simul. **9**, 59 (2011).

[14] T. Duguet, Y. Han, C. Yuen, D. Jing, B. Ünal, J. W. Evans, and P. A. Thiel, Proc. Nat. Acad. Sci. **108**, 989 (2011).

[15] Y. Han, B. Ünal, D. Jing, P. A. Thiel, and J. W. Evans, J. Chem. Phys. **135**, 084706 (2011).

[16] Y. Han, D. Jing, B. Ünal, P. A. Thiel, and J. W. Evans, Phys. Rev. B **84**, 113414 (2011).

[17] R. Ferrando, F. Hontinfinde, and A. C. Levi, Phys. Rev. B **56**, R4406 (1997).

[18] C. Mottet, R. Ferrando, F. Hontininde, and A. C. Levi, Surf. Sci. **417**, 220 (1998).

[19] C. D. Giorgi, P. Aihemaiti, F. B. de Mongeot, C. Boragno, R. Ferrando, and U. Valbusa, Surf. Sci. **487**, 49 (2001).

[20] The edge diffusion barrier on $\langle \bar{1}10 \rangle$ edges is $E_e^\parallel = E_d^\parallel - E_b^\perp + 2E_b'^\perp = E_d^\parallel + |E_b^\perp| - 2|E_b'^\perp|$, which can be comparable to $E_d^\parallel$, in contrast to the higher initial value approximation value.

[21] Y. Han, J. Y. Zhu, F. Liu, S.-C. Li, J.-F. Jia, Y.-F. Zhang, and Q.-K. Xue, Phys. Rev. Lett. **93**, 106102 (2004).

[22] M. Li, C. Z. Wang, J. W. Evans, M. Hupalo, M. C. Tringides, and K. M. Ho, Phys. Rev. B **79**, 113404 (2009).

[23] Y. Yao, Ph. Ebert, M. Li, Z. Zhang, and E. G. Wang, Phys. Rev. B **66**, 041407 (2002). Note the typographic error in the expressions for equilibrium adatom densities at island edges.

[24] In this traditional macroscopic setting, the characteristic length describing the surface morphology is assumed to far exceed any microscopic length scales.

[25] J. W. Evans, P. A. Thiel, and M. C. Bartelt, Surf. Sci. Rep. **61**, 1 (2006).

[26] COMSOL Multiphysics (formerly FEMLAB) is a finite element analysis, solver, and simulation software developed by Comsol, Inc. (www.comsol.com).

[27] FEMLAB analysis finds $K_{rBCF,1R} = 0.00147$ nm^2/s, $K_{rBCF,1L} = 0.00073$ nm^2/s; $K_{rBCF,2R} = -0.00157$ nm^2/s; $K_{rBCF,3R} = -0.00462$ nm^2/s, $K_{rBCF,3L} = 0.00020$ nm^2/s; $K_{rBCF,4R} = 0.00046$ nm^2/s, $K_{rBCF,4L} = 0.00448$ nm^2/s; $K_{rBCF,5R} = -0.00004$ nm^2/s, $K_{rBCF,5L} = -0.00115$ nm^2/s; $K_{rBCF,6L} = 0.00079$ nm^2/s; and $K_{rBCF,7R} = -0.00115$ nm^2/s. Here $K_{rBCF,jR(L)}$ denotes the integrated flux for the right (left) end of island j, and a $+(-)$ sign corresponds to decay (growth).

[28] R. E. Caflisch, W. E, M. F. Gyure, B. Merriman, and C. Ratsch, Phys. Rev. E **59**, 6879 (1999).

[29] R. E. Caflisch and D. Margetis, Multiscale Model. Simul. **7**, 242 (2008).

[30] O. Pierre-Louis and M. I. Haftel, Phys. Rev. Lett. **87**, 048701 (2001).

[31] Decompose $J_y = J_{y,attach} - J_{y,detach}$, where $J_{y,detach} = h_{det}n_{edge}$ with $h_{det} \equiv \nu e^{-\beta E_{det}^\perp}$ and $E_{det}^\perp = E_d^\perp - E_b^\perp$. Define $L_{cr}^\parallel \equiv 2bh_{cr}/h_{det}$ as a characteristic length for corner rounding in competition with detachment. Then, if that n_{edge} is effectively uniform due to rapid edge diffusion integrating Eq. (9) and using Eq. (10) yields $n_{edge} \approx \frac{(1-p_{cr})J_{y,attach}}{h_{det}} + p_{cr}e^{-\beta E_b^\perp}n_{001}$, where $p_{cr} = L_{cr}^\parallel/(L^\parallel + L_{cr}^\parallel)$ measures the efficiency of corner rounding.

[32] An alternative formulation of BC for $\langle 001 \rangle$ ends of islands (cf. Ref. 13) sets $n_{001} = 1$ at the island ends, but then the rate for detachment from these $\langle 001 \rangle$ that ends in the x direction is $e^{-\beta E_{form}}h^\parallel$, and there are related modifications for corner rounding.

[33] We can mimic this picture by setting $c_r = 0$. This produces a much lower decay rate $K_{DDE} = 0.0248h^\parallel n_\infty$ and large one-way corner-rounding flux $J_{cr}/K_{DDE} = +1.55$ determined from $n_{corner}^\dagger = 1.018$.

[34] Y. Li, M. C. Bartelt, J. W. Evans, N. Waelchli, E. Kampshoff, and K. Kern, Phys. Rev. B **56**, 12539 (1997).

[35] $K_{DDE} = 0.0472\ h^\parallel n_\infty$ is obtained in a rBCF model with $E_b^\perp = 0$, $h_{cr} = h^\perp$ and $c_r = 1$.

[36] For marginal misalignment ($j_{R1} = 4$, $j_{R2} = 15$, $j_{L1} = 14$, $j_{L2} = 21$, and $j_M = 24$), we find that $K_{DDE} = 0.0142\ h^\parallel n_\infty$. For complete misalignment ($j_{R1} = 4$, $j_{R2} = 15$, $j_{L1} = 16$, $j_{L2} = 23$, and $j_M = 26$), we find that $K_{DDE} = 0.0087\ h^\parallel n_\infty$.

[37] Y. Han, B. Unal, F. Qin, D. Jing, C. J. Jenks, D. J. Liu, P. A. Thiel, and J. W. Evans, Phys. Rev. Lett. **100**, 116105 (2008).